Magnetic properties of vacancies in graphene and single-walled carbon nanotubes

Yuchen Ma, P O Lehtinen, A S Foster and R M Nieminen

Laboratory of Physics, Helsinki University of Technology, PO Box 1100, Helsinki 02015, Finland
E-mail: yma@fyslab.hut.fi, www.fyslab.hut.fi

Abstract. Spin-polarized density functional theory has been used to study the properties of vacancies in a graphene sheet and in single-walled carbon nanotubes (SWNTs). For graphene, we find that the vacancies are magnetic and the symmetry of the sheet is broken by the distortion of an atom next to the vacancy site. We also studied vacancies in four armchair SWNTs from (3,3) to (6,6) and six zigzag SWNTs from (5,0) to (10,0). Our calculations demonstrate that vacancies can change the electronic structure of SWNTs, converting some metallic nanotubes to semiconductors and vice versa. Metallic nanotubes with vacancies exhibit ferro- or ferrimagnetism, whereas some semiconducting nanotubes with vacancies show an antiferromagnetic order. The magnetic properties depend on chiralities of the tubes, the configuration of the vacancy and the concentration of the vacancies.

Contents

Institute *of* **Physics** Φ DEUTSCHE PHYSIKALISCHE GESELLSCHAFT

1. Introduction

It has been verified both by experiments [1]–[3] and by theory [4]–[8] that carbon materials can exhibit magnetism without impurities. The technological uses of controllable magnetic carbon systems are extensive, and it is crucial to understand the mechanism in detail. However, the specific source of the magnetism observed in experiments is still a subject of debate, with several possible alternatives. Rhombohedral C_{60} (Rh-C_{60}) exhibits some typical features of ferromagnets [1, 9]—this has been attributed to vacancy defects and the interplay between these defects and sp^3 hybridization. Peculiar localized states have been found to exist at the zigzag edge of finite graphite sheets [4, 5] and at the end of zigzag single-walled carbon nanotubes (SWNTs) [10], and these localized edge states probably induce magnetic polarization. Even for systems with no under-coordinated carbon atoms, carbon radicals could be the source of magnetism [7]. In each case, it is necessary to consider whether intrinsic carbon defects are responsible for the magnetism observed—an aim we pursue in this paper.

During the growth process and under ion irradiation, defects will be introduced in graphite and carbon nanostructures [11, 12]. Adatom interstitial–vacancy pairs are the dominant defect species, and it is important to understand their general properties. In this paper, we focus on the properties of graphite and carbon nanotubes, which are both intrinsically important and good examples of carbon systems. Recent calculations have shown that the carbon adatom defects on a graphene sheet and on nanotubes both have a magnetic moment [6, 8]. This is supported by experiments suggesting the presence of localized spin moments in carbon nanotubes [13, 14], probably related to dangling bonds on the surface. For nanotubes, studies have shown [8] that the magnitude of the adatom magnetic moment depends on the radii and chiralities of the nanotubes. Previous studies of vacancies in carbon nanotubes [15] using the tight-binding method did not consider spin polarization. To understand how the adatom–vacancy defect pair contributes, in total, to the magnetism of carbon systems, it is necessary to consider the properties of vacancies in graphite and carbon nanotubes. This is undertaken in the present work.

2. Methods

The calculations have been performed using the periodic plane wave VASP [16, 17] code, implementing the spin-polarized density functional theory (DFT) and the generalized gradient approximation of Perdew *et al* [18]. We have used projected augmented wave potentials [19, 20] to describe the core ($1s^2$) electrons, with the $2s^2$ and $2p^2$ electrons of carbon considered as valence electrons. A kinetic energy cutoff of 400 eV is found to converge the total energy to within 1 meV. Brillouin zone sampling is performed using the k-point generation scheme of Monkhorst and Pack [21] (the Γ-point is included). Five k-points for the graphene sheet and four k-points for the nanotubes were found to be sufficient to obtain an meV convergence of the total energy. The minima of the total energy were found using a conjugate gradient (CG) algorithm. All atoms are fully relaxed until the change in energy upon ionic displacement is below 0.1 meV.

This method has been shown previously to give good accuracy for this type of carbon system [6]. We model graphite as a single graphene sheet, since the weak van der Waals interaction between layers does not significantly affect intralayer processes. Note that, for bulk graphite, the present method does give a layer separation within 4% of the experiment, yet the agreement is fortuitous, since DFT does not reproduce the real interlayer van der Waals interactions [22].
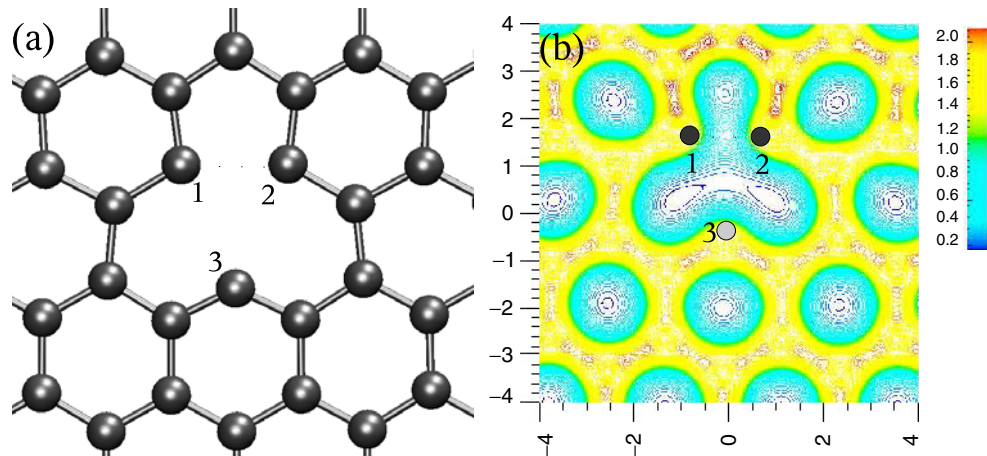
Figure 1. (a) Atomic structure of the vacancy in the graphene plane; (b) charge density of the vacancy in the graphene plane (e/Å^3).

However, as long as we avoid interlayer processes, this system provides a very good model for graphite.

3. Results

3.1. Vacancy on a graphene sheet

Using the Hückel method, Hjort *et al* [23] suggested that the three symmetric atoms neighbouring the vacancy on a graphite surface can contribute an extra π electron to the system, which may give rise to an unpaired spin, i.e. the vacancy would be magnetic. However, previous finite-cluster DFT calculations for the vacancy in graphene [24, 25] predicted that it undergoes a Jahn–Teller distortion, breaking the symmetry of the graphene sheet and providing a nonmagnetic solution.

To study the properties of the vacancy, we consider a graphene sheet of 128 atoms with a single carbon atom removed. We find that the vacancy does undergo a Jahn–Teller distortion after relaxation, since two of the atoms closest to the vacancy (atoms 1 and 2 in figure 1(a)) move closer, forming a pentagon-like structure and the final atom (atom 3 in figure 1(a)) is displaced by 0.18 Å out of the plane. The formation energy (calculated in the same way as in [26]) of the vacancy was 7.7 eV, which compares well with the experimental value of 7.0 ± 0.5 eV [27] and with the previous DFT values of 7.6 eV [28] and 7.4 eV [24]. We found that the formation energy of the 128-atom sheet converged to within 0.02 eV with respect to the system size. Atoms 1 and 2 form an extended C–C bond with a length of 2.02 Å in comparison with the standard length of 1.42 Å for graphene. The charge density seen in figure 1(b) around the vacancy demonstrates clearly the increase in density between atoms 1 and 2, indicating the formation of a weak covalent bond.

The ground state of the vacancy is spin-polarized with a magnetic moment of $1.04\mu_B$, and the spin density is shown in figure 2. After the removal of one atom, each of the three neighbouring atoms now has one sp^2 dangling bond. Formation of the pentagon saturates two of these bonds, but the remaining unsaturated bond is responsible for the magnetic moment (i.e. the dangling bond on atom 3 seen in figure 2). In tests with smaller 50- and 98-atom graphene sheets, we found that, despite size constraints, conditions were still energetically favourable for the formation of the pentagon and that the vacancy was magnetic.
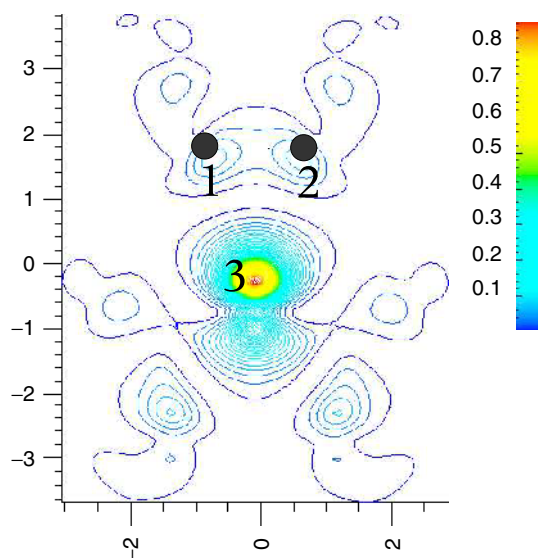
Figure 2. Spin density of the vacancy in the graphene plane (e/Å^3).

Compared with recent DFT calculations of the vacancy by local-density approximation (LDA) [24, 25], our calculations show some significant differences. Those two studies considered the vacancy both in a finite, hydrogen-terminated graphene cluster and in a periodic graphene sheet, with both systems exhibiting a nonmagnetic vacancy. In the periodic calculations [24], the authors considered a 63-atom unit cell. Our spin-polarized calculations with the 50-atom cell show that neither the formation energy nor the magnetic moment are converged well for this system size, indicating that there is significant defect–defect interaction. For the finite cluster approach, it is more difficult to compare results, but the fact that the authors considered only fixed-spin systems [24] in the LDA calculations probably restricted their possible solutions. Comparing the atomic structures of the vacancy, we also find differences. Although all the calculations agree that a Jahn–Teller distortion occurs, El-Barbary *et al* [24] report a displacement of atom 3 out of the plane by about 0.47 Å, which is much larger than the 0.18 Å we observed. However, if we restrict our system to an equal spin-up and spin-down density solution, we find a nonmagnetic ground-state about 0.1 eV higher in energy, with an atom 3 displacement of 0.46 Å. This implies that, although our methods basically agree with previous studies, subtle finite-cluster or fixed-spin effects were responsible for the nonmagnetic ground state in their calculations.

3.2. Vacancies on nanotubes

Different from the simple sp^2 bonds in graphite, the bonds in carbon nanotubes are of sp^2–sp^3 character, and the hybridization of σ, σ^*, π and π^* orbitals can be quite large, especially for small-diameter SWNTs [29]. Thus the magnetic properties of vacancies on SWNTs will be more complicated, and will have a close relation to the radii and chiralities of the SWNTs. The concentration of vacancies also affects the properties of nanotubes. Hence, in this paper, we consider not only different radii and chiralities but also various vacancy concentrations of some SWNTs as examples.

Carbon nanotubes are formed by the seamless rolling of graphite sheets over themselves [30]. The structure of a nanotube is usually characterized by the chiral vector (n,m). Tubes designated by $(n,0)$ and (n,n) are termed 'zigzag' and 'armchair' tubes, respectively. The properties of
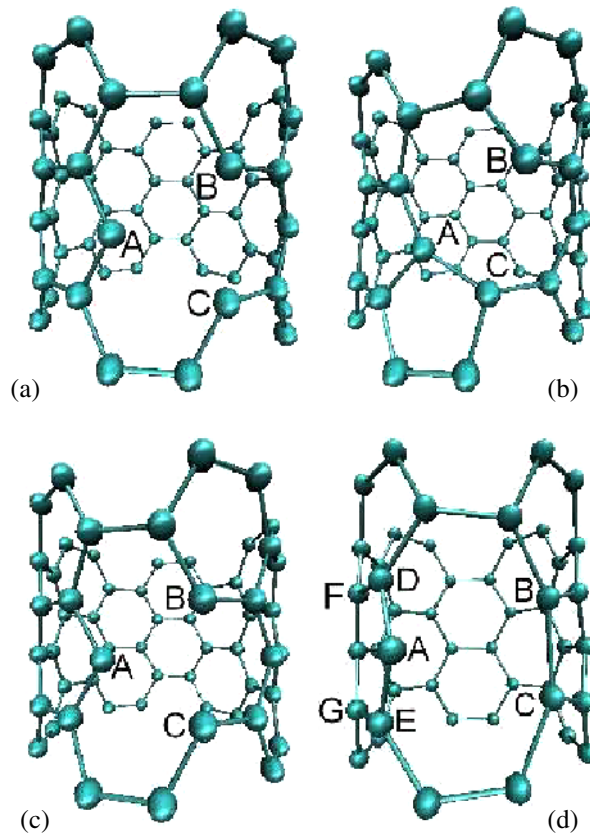
Figure 3. Vacancy structures on the armchair SWNT: (a) unreconstructed structure, (b) ground state—'perpendicular' configuration, (c) metastable state of the (5,5) and (6,6) tubes—'parallel' configuration, (d) metastable state of the (3,3) and (4,4) tubes—'parallel' configuration.

carbon nanotubes have a close relation to the chiralities. For example, if $n - m$ is divisible by 3, the tube is a metal, otherwise it is semiconducting. Four armchair SWNTs (3,3), (4,4), (5,5) and (6,6) and six zigzag SWNTs (5,0), (6,0), (7,0), (8,0), (9,0) and (10,0) are studied here. The supercells were constructed with adequate empty space in the radial direction of the tubes to avoid interaction between adjacent tubes. Periodical boundary conditions are applied in the axial direction. There is only one vacancy in the unit cell, and different vacancy concentrations are simulated by using different lengths of the unit cells along the axial direction of the tubes. To avoid confusion, the term *linear density of vacancies* will be used instead of the term *concentration* in the following discussion. A small segment length means high linear density. The length of the unit cell is represented by the number of carbon rings in the corresponding perfect SWNT. Each carbon ring on the perfect $(n,0)$ SWNT and (n,n) SWNT consists of $2n$ and $4n$ atoms respectively. The minimal length is six rings for the zigzag tubes and five rings for most of the armchair tubes.

Different from graphite, the three two-coordinated atoms surrounding the unreconstructed vacancy on the wall of the SWNT can be classified into two groups. For armchair SWNTs, atoms B and C in figure 3(a) are equivalent. For zigzag SWNTs, atoms B and C in figure 4(a) are equivalent. Note that the energy landscape for different vacancy configurations is quite complex, and several metastable states exist [31] during the creation and migration processes. We find that
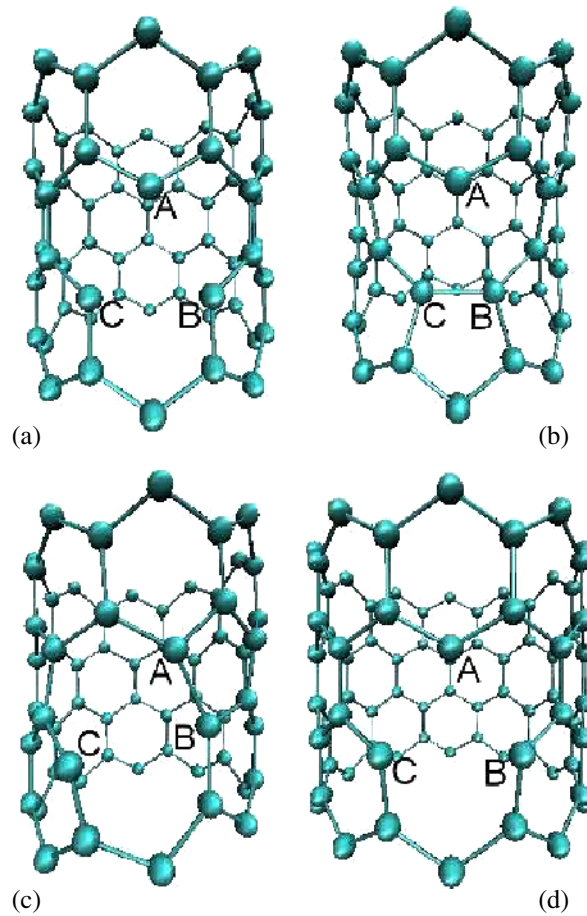
Figure 4. Vacancy structures on the zigzag SWNT: (a) unreconstructed structure, (b) ground state—'perpendicular' configuration, (c) one metastable state—'parallel' configuration, (d) one metastable state of the (5,0) and (10,0) tubes—'3db' configuration.

just removing a carbon atom and relaxing with CG technique could not always result in the true ground state of the vacancy. Therefore, for all the ten SWNTs studied, several configurations have to be considered.

For the armchair SWNTs, the ground state of the vacancy is as shown in figure 3(b). The new bond A–C in the pentagon is in the range 1.52–1.57 Å. The possible metastable state is one where atoms B and C form a bond. For the (3,3) and (4,4) tubes, the length of the bond B–C is 1.69 and 1.76 Å, respectively (see figure 3(d)). However, for the (5,5) and (6,6) tubes, the distance between atoms B and C is 2.20 Å (see figure 3(c)), and the interaction between them is very weak. For the six zigzag SWNTs, the ground state of the vacancy is as shown in figure 4(b), with the new bond B–C in the range 1.45–1.55 Å. One possible metastable state is shown in figure 4(c), where atoms A and B form a bond with the bond length ranging from 1.64 to 1.72 Å. For the (5,0) and (10,0) tubes, there is another possible metastable state as shown in figure 4(d), where the three dangling bonds remain. In fact, direct CG minimization from the unreconstructed vacancy structure will result in the structure shown in figure 4(d) for the (5,0) and (10,0) tubes and the structure shown in figure 4(b) for the other zigzag tubes from (6,0) to (9,0). According to the direction of the new bond in the pentagon relative to

Table 1. Properties of 5-ring armchair SWNTs with vacancies of different configurations.

Nanotube	Configuration	E_F (eV)	Class	Magnetic moments (μ_B)
(3,3)	Perpendicular	4.4	Semiconductor	0.0
	Parallel	5.2	Metal	1.0
(4,4)	Perpendicular	5.3	Semiconductor	0.0
	Parallel	6.2	Metal	1.0
(5,5)	Perpendicular	5.6	Metal	0.6
	Parallel	7.1	Semiconductor	0.0
(6,6)	Perpendicular	5.9	Semiconductor (metal)[a]	0.0 (0.4)[a]
	Parallel	7.3	Semiconductor	0.0

[a] 4-ring (6,6) tube.

Table 2. Properties of 6-ring zigzag SWNTs with vacancies of different configurations.

Nanotube	Configuration	E_F (eV)	Class	Magnetic moments (μ_B)
	Perpendicular	4.6	Semiconductor	0.0
(5,0)[a]	Parallel	5.1	Semiconductor	0.0[b]
	3db	6.0	Semiconductor	0.0[b]
(6,0)	Perpendicular	5.0	Metal	0.3
	Parallel	5.8	Metal	0.9
(7,0)	Perpendicular	5.2	Semiconductor	0.0
	Parallel	6.3	Metal	0.8
(8,0)	Perpendicular	5.3	Semiconductor	0.0
	Parallel	6.5	Metal	0.8
(9,0)	Perpendicular	5.4	Semiconductor	0.0
	Parallel	6.4	Metal	1.0
	Perpendicular	5.5	Semiconductor	0.0
(10,0)	Parallel	6.7	Metal	0.9
	3db	7.4	Metal	1.9

[a] 8-ring (5,0) tube.
[b] Antiferromagnetic.

the axis of the tube, we define the configuration in figures 3(b) and 4(b) as 'perpendicular', whereas those in figures 3(c), (d) and 4(c) as 'parallel' configurations. The configuration in figure 4(d) is defined as '3db' (three dangling bonds). Detailed information on each configuration of all the tubes is given in tables 1 and 2.

3.2.1. Armchair nanotubes. For the 5-ring armchair SWNTs, only the 'parallel' configurations on the (3,3) tube (denoted as 'parallel' (3,3) below) and the (4,4) tube and the 'perpendicular' configurations on the (5,5) tube (denoted as 'perpendicular' (5,5) below) exhibit magnetism,
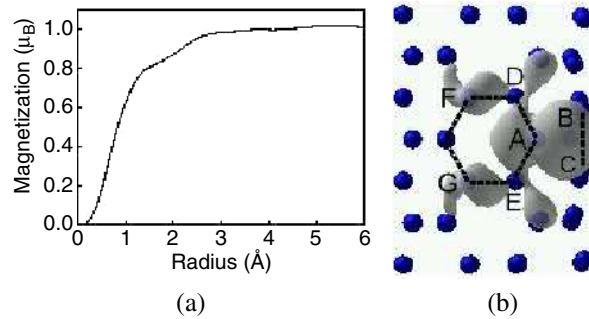
Figure 5. (a) Magnetization profile as a function of the integration radius R_i around the two-coordinated atom, and (b) isosurface of the magnetization density from a direction normal to the axis of the tube at $0.01\mu_B\,\text{Å}^{-3}$ on the 5-ring (4,4) SWNT with vacancy of 'parallel' configuration.

with magnetic moments of 1.0, 1.0 and $0.6\mu_B$, respectively. After testing with unit cells of different lengths ranging from 5 to 8 rings, we find that magnetic properties of the 'parallel' (3,3) and 'parallel' (4,4) tubes are independent of linear density of the vacancies. The interaction between the spins in adjacent supercells is very small—the magnetic moments are highly localized. This can be seen from figure 5(a), which gives the distribution of magnetization around the two-coordinated atom A on the 5-ring (4,4) tube displayed in figure 3(d). The magnetization around one atom placed at $\mathbf{R_0}$ is calculated as

$$M(R_i) = \int_{\Omega_{R_i}} [n_\uparrow(\mathbf{r} - \mathbf{R_0}) - n_\downarrow(\mathbf{r} - \mathbf{R_0})]\,d\mathbf{r},$$

where Ω_{R_i} is a sphere of radius R_i and $n_\uparrow$ and $n_\downarrow$ are the charge densities for the spin-up and spin-down electrons, respectively. In figure 5(a), the magnetization has saturated for $R_i = 3\,\text{Å}$. The spin polarization beyond this range is very small. This radius is much less than the minimal length of the unit cells that we use for the (4,4) tube. Figure 5(b) depicts the isosurface of the magnetization density $\Delta n(\mathbf{r})$ on the 5-ring (4,4) tube from the side, where the magnetization density is defined as $\Delta n(\mathbf{r}) = n_\uparrow(\mathbf{r}) - n_\downarrow(\mathbf{r})$. The distribution of the magnetization around the two-coordinated atom resembles an unsaturated σ dangling bond. From figures 5(a) and (b), we can conclude that it is mainly the unpaired σ electron that contributes to the magnetic moment. The distribution of the magnetization is very similar to that of the 128-atom graphene sheet (cf figures 2 and 5(b)). It appears that chirality has no influence on the magnetic properties of the 'parallel' (3,3) and 'parallel' (4,4) tubes. This is due to the special atomic structures around the vacancies. On these two tubes, the two-coordinated carbon atom A and its two nearest-neighbour atoms, D and E, as well as the two next-neighbour atoms in the same hexagon, F and G, are nearly coplanar (see figure 3(d)). The local curvature at atom A is almost 0, and the hybridization of the σ and π orbitals is very small. The π-electron network on the wall of the (3,3) and (4,4) tubes has been hardly disturbed by the σ-electron spin polarization. This explains the localization of the magnetic moments.

The magnetic property of 'perpendicular' armchair SWNT depends on the chirality of the tube and the linear density of the vacancies. Only the 5-ring (5,5) tube and the 4-ring (6,6) tube exhibit magnetic moments of 0.6 and $0.4\mu_B$, respectively. For longer (5,5) and (6,6) tubes, no
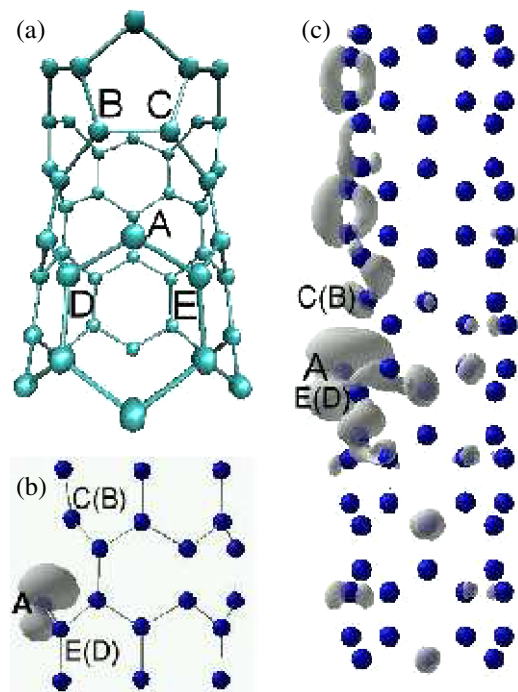
Figure 6. (a) 'Perpendicular' vacancy structure on the (6,0) SWNT. The isosurfaces of the magnetization density at (b) $0.04\mu_B\,\text{Å}^{-3}$ and (c) $0.0027\mu_B\,\text{Å}^{-3}$ from the side view of the 10-ring (6,0) SWNT.

magnetic moment was observed. Both the σ electron of the dangling bond and the π electrons have contributed to the magnetic polarization.

3.2.2. Zigzag nanotubes. The ground state of the vacancy on the zigzag SWNT, the 'perpendicular' configuration, is nonmagnetic, except for the (6,0) tube. The magnetic property of the 'perpendicular' (6,0) tube depends on the linear density of vacancies. The magnetic moments of the 6-ring, the 8-ring and the 10-ring 'perpendicular' (6,0) tubes are 0.3, 0.7 and $0.5\mu_B$, respectively. Figure 6(b) depicts the isosurface of the magnetization density on the 10-ring (6,0) tube at a density value of $0.04\mu_B\,\text{Å}^{-3}$ from the side. The spin polarization comes from both the σ and π electrons. There is some hybridization between the σ and π orbitals around the two-coordinated atom A. Since the π electrons on the SWNT are delocalized, the magnetization of the (6,0) tube with vacancies is also delocalized. This explains the dependence of magnetic properties of the (6,0) tube on the linear density of the vacancies. Figure 6(c) shows the isosurface of the magnetization density at the density value of $0.0027\mu_B\,\text{Å}^{-3}$ for the 10-ring tube. We can see that spin-polarized π electrons are distributed along the whole tube. The local magnetic moment at atom A is $0.27\mu_B$, and the remaining $0.24\mu_B$ magnetic moment arises from these π electrons. The local magnetic moments at atom A are 0.15 and $0.25\mu_B$ for the 6- and 8-ring (6,0) tubes, respectively. It seems that the local magnetic moment at atom A has a saturation value of about $0.27\mu_B$.

The 'parallel' metastable state is magnetic for all the zigzag SWNTs from (5,0) to (10,0). However, the (5,0) tube is antiferromagnetic, i.e. the positive and negative magnetizations reside on different atoms and the net magnetic moment of the unit cell is zero. The other tubes exhibit
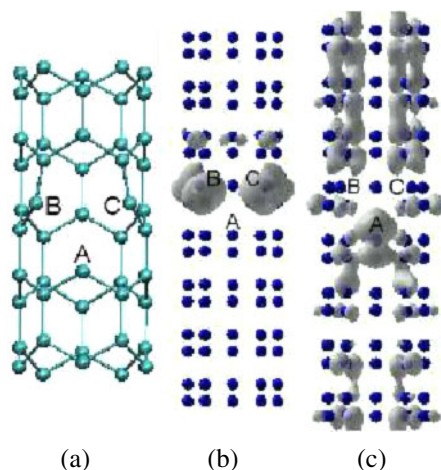
Figure 7. (a) '3db' vacancy structure on the (5,0) SWNT. The isosurfaces of the magnetization density at $0.009\mu_B \text{Å}^{-3}$ (b) and $-0.004\mu_B \text{Å}^{-3}$ (c) on the 8-ring (5,0) SWNT.

ferromagnetism with magnetic moment around $1.0\mu_B$. By analysing the distribution of the magnetization density, we found that the magnetic properties of the 'parallel' tubes from (6,0) to (10,0) are very similar to that of the 'parallel' (4,4) tube. It is mainly the unpaired σ electron that contributes to the magnetic moment and the magnetization is highly localized.

As for the 'parallel' (5,0) tube, the (5,0) tube having the '3db' vacancy also exhibits antiferromagnetism. In this paper, we use the '3db' (5,0) tube as an example to describe the antiferromagnetism. For shorter '3db' (5,0) tubes, such as the 6-ring tube, despite the fact that the magnetization density distribution still shows an antiferromagnetic order, the local magnetic moment is very low, two orders of magnitude lower when compared with the 8-ring tube. Hence, the 6-ring '3db' (5,0) tube may be considered to be nonmagnetic. Figure 7(b) shows the iso-surface of magnetization density at the density value of $0.009\mu_B \text{Å}^{-3}$ on the 8-ring (5,0) tube. The positive magnetization comes mainly from the σ electrons of the two dangling bonds. A large part of the positive magnetization accumulates around atoms B and C in figure 7. The contribution of π electrons to positive magnetization is negligible. The local magnetic moments at atoms B and C are both $0.14\mu_B$. At atom A, the magnetization is negative and its distribution is similar to that shown in figure 6(b) for the (6,0) tube. However, the local magnetic moment at atom A is $-0.07\mu_B$, which is only a small fraction of the total negative magnetization. The remaining negative magnetization (more than $-0.21\mu_B$) belongs to the π electrons on the wall of the tube, as seen from figure 7(c). π-Electron spin polarization plays an important role in the magnetization. This implies that the magnetic properties of the (5,0) tube may have a close relation to the linear density of the vacancies. In fact, for both the 10-ring and the 12-ring (5,0) tubes, the magnitudes of local magnetic moments at atoms A, B and C became -0.14, 0.28 and $0.28\mu_B$, respectively. It seems that the local magnetic moments at these three atoms have reached their saturation values for the 10-ring tube. The positive magnetization of the 'parallel' (5,0) tube comes mainly from the σ electron of the dangling bond, whereas the negative one comes entirely from the π electrons.

The (10,0) tube with '3db' vacancy exhibits something like ferrimagnetism, with a net magnetic moment of $1.9\mu_B$. Figures 8(a) and (b) show the isosurfaces of the magnetization
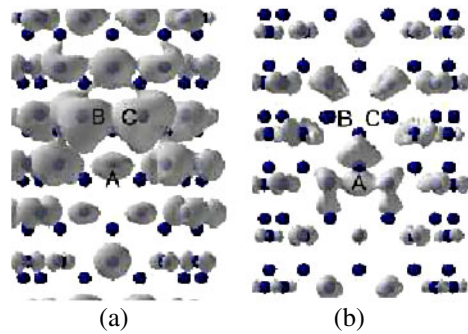
Figure 8. The isosurfaces of the magnetization density at $0.003\mu_B\,\text{Å}^{-3}$ (a) and $-0.003\mu_B\,\text{Å}^{-3}$ (b) on the 6-ring (10,0) SWNT with vacancy of '3db' configuration.

densities at the density values of 0.003 and $-0.003\mu_B\,\text{Å}^{-3}$, respectively. Positive magnetization comes both from the σ electrons of the dangling bonds of atoms B and C and from the π electrons. Negative magnetization arises both from the σ electrons of the dangling bonds of atom A and from the π electrons. Atoms B and C only contribute to the positive magnetization, whereas atom A contributes to both the negative (see figure 8(b)) and positive magnetizations (see figure 8(a)). The local magnetic moments at atoms A, B and C are -0.10, 0.40 and $0.40\mu_B$, respectively. The adjacent atoms on the wall of the perfect nanotube belong to different sublattices. Comparing figures 8(a) and (b), we can see that the positive and negative magnetizations of the π electrons reside on different sublattices. The magnitudes of these magnetization on different sublattices are different. Therefore this tube has a ferrimagnetic structure.

4. Discussion

Armchair SWNTs are predicted to be metallic and this has been verified by experiments and first-principles calculations [32]–[34]. A simple graphene sheet model predicts that zigzag SWNTs with indices $(3m,0)$ would be metallic, where m is an integer. However, previous experiments [32] have shown that (9,0), (12,0) and (15,0) SWNTs have small energy gaps. Ouyang *et al* [32] has generalized that the energy gaps of the $(3m,0)$ zigzag tubes would scale as R^{-2}, where R is the tube radius. Thus these zigzag tubes are, in fact, small-gap semiconductors and are not metallic. This is consistent with theoretical calculations [29, 35, 36]. However, calculations based on local density functional theory showed that the (6,0) SWNT is metallic [29, 33]. Recent calculations have also predicted the metallic character of the (5,0) tube [33, 34]. We have calculated the band structures of the 10 SWNTs studied and found that the perfect (3,3), (4,4), (5,5), (6,6), (5,0) and (6,0) tubes are metallic, whereas the (7,0), (8,0), (9,0) and (10,0) tubes are semiconductors. The energy gap of the (9,0) tube was calculated to be 0.16 eV, which is in agreement with the value of 0.17 eV obtained by Blase *et al* [29] and compares well with the experimental value of 0.08 eV [32].

Furthermore, we calculated the electronic structures of the SWNTs having vacancies. The results are given in tables 1 and 2. Vacancies can convert both metallic nanotubes into semiconductors and semiconducting ones into metals. For most of the SWNTs, the electronic properties are strongly dependent on the vacancy configuration. Only the (5,0) and (6,0) tubes are
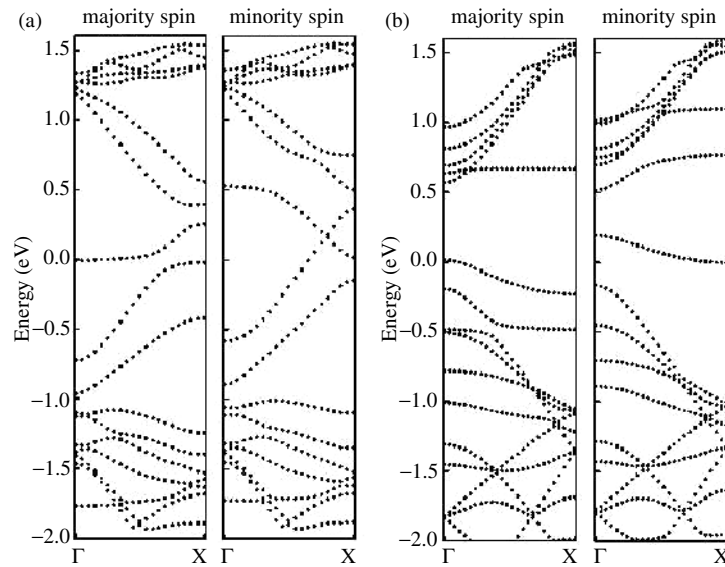
Figure 9. The band structures for the 5-ring (5,5) SWNT with vacancy of 'perpendicular' configuration (a) and the 6-ring (10,0) SWNT with vacancy of '3db' configuration (b) ($E_F = 0$).

always semiconducting and metallic, respectively. We conclude also that only metallic SWNTs with vacancies could exhibit ferromagnetism or ferrimagnetism.

It is predicted that peculiar localized states exist at the edges of H-terminated graphitic ribbons [4, 37]. These edge states originate from the π orbitals of the carbon atoms. If the edges are zigzag, these edge states produce a flat band at the Fermi level. The presence of the flat band leads to electron–electron interactions, which in turn lead to magnetic polarization with moments localized at the zigzag edges [4, 37, 38]. It is the π electrons that contribute to this magnetic polarization. The vacancy on the SWNT acts like a zigzag edge. We expect that peculiar edge states may exist around the vacancies in the magnetic SWNTs having vacancies, and some flat bands may also appear at the Fermi level. However, because of the curvature of the SWNT, hybridization of the σ and π orbitals and the presence of the dangling bonds at the vacancies, such characteristics may not be evident. Vacancy concentration also influences the appearance and flatness of the flat band, similar to the influence of width of the zigzag graphene ribbons on the flat band [37, 39]. As examples, figure 9 shows the band structures of the 5-ring 'perpendicular' (5,5) and the 6-ring '3db' (10,0) tubes. For the '3db' (5,0) tube, a flat band appears near the Fermi level (at -0.07 eV for the 8-ring tube, setting $E_F = 0.0$). The band is almost dispersionless along the whole Γ–X direction. This flat band is nearly degenerate, i.e. the splitting between the spin-up and spin-down branches is very small. The tubes with flat bands are those where π electrons play an important role in the magnetic polarization. These observations suggest that the generalized flat-band theory of magnetism [40] may partly explain the origin of magnetic polarization on the SWNTs having vacancies.

Scanning tunneling microscopy (STM) is an important tool to study vacancies on graphite and nanotubes [41]–[44]. It has been predicted that the vacancy could result in a sharp increase in the local density of states (LDOS) near the Fermi level (E_F) on atoms closest to the vacancy [43, 44]. We also investigated the LDOS of one nonmagnetic tube and one magnetic tube, as
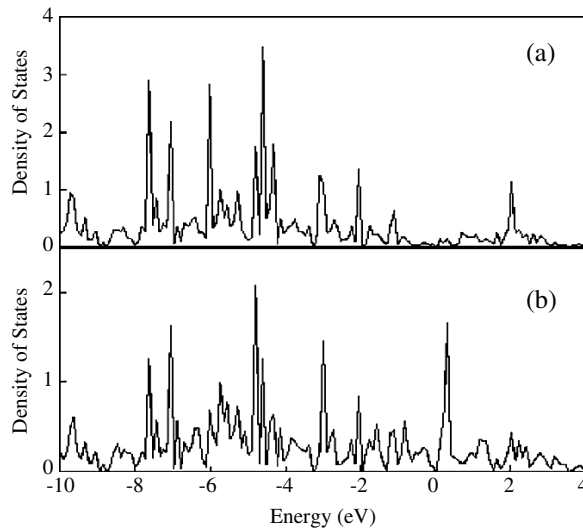
Figure 10. (a) LDOS on four adjacent atoms far away from the vacancy and (b) three atoms surrounding the vacancy for the 6-ring (7,0) SWNT having vacancy of 'perpendicular' configuration ($E_F = 0$).
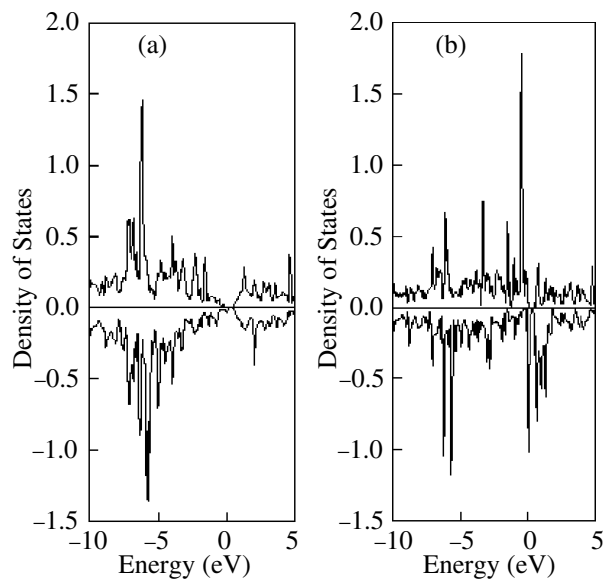

Figure 11. LDOS on four adjacent atoms far away from the vacancy (a) and the LDOS on the three atoms surrounding the vacancy (b) for the 6-ring (10,0) SWNT with vacancy of '3db' configuration. Positive and negative LDOSs are for the spin-up and the spin-down electrons, respectively ($E_F = 0$).

shown in figure 10 for the 6-ring 'perpendicular' (7,0) tube and in figure 11 for the 6-ring '3db' (10,0) tube. Figures 10(b) and 11(b) show the LDOS on the three atoms surrounding the vacancy, whereas figures 10(a) and 11(a) show the LDOS on four adjacent atoms (one atom is bonded to the other three atoms) far away from the vacancy. For the (7,0) tube, the LDOS has a sharp

increase just above E_F. For the (10,0) tube, there are also sharp increases in LDOS near E_F for both the spin-up and the spin-down electrons. Such sharp increases in LDOS are absent near E_F for atoms far away from the vacancy and, hence, the vacancy will result in a protrusion in the STM image (assuming imaging with small bias).

5. Summary

In conclusion, we have calculated the magnetic properties of single vacancies in a graphene sheet and ten small-diameter SWNTs using first-principles methods. The dependence of the magnetic properties on the chiralities of the tubes, configuration of the vacancy and vacancy concentrations has been demonstrated. A vacancy can change the electronic structure of the nanotube—a vacancy can convert both metallic nanotubes into semiconductors and semiconducting ones to metals. If the nanotube is metallic after the introduction of a vacancy, the nanotube will be ferromagnetic or ferrimagnetic. Semiconducting (5,0) tubes with certain kinds of vacancies can exhibit antiferromagnetism.

Acknowledgments

References

[1] Makarova T L, Sundqvist B, Höhne R, Esquinazi P, Kopelevich Y, Scharff P, Davydov V A, Kashevarova L S and Rakhmanina A V 2001 *Nature* **413** 716
[2] Narlikar A (ed) 2003 *Studies of High-Temperature Superconductivity* vol 45 (New York: Nova Science) ch 7, p 107
[3] Coey J M D, Venkatesan M, Fitzgerald C B, Douvalis A P and Sanders I S 2002 *Nature* **420** 156
[4] Fujita M, Wakabayashi K, Nakada K and Kusakabe K 1996 *J. Phys. Soc. Japan* **65** 1920
[5] Shibayama Y, Sato H, Enoki T and Endo M 2000 *Phys. Rev. Lett.* **84** 1744
[6] Lehtinen P O, Foster A S, Ayuela A, Krasheninnikov A, Nordlund K and Nieminen R M 2003 *Phys. Rev. Lett.* **91** 017202
[7] Park N, Yoon M, Berber S, Ihm J, Osawa E and Tománek D 2003 *Phys. Rev. Lett.* **91** 237204
[8] Lehtinen P O, Foster A S, Ayuela A and Nieminen R M 2004 *Phys. Rev.* B **69** 155422
[9] Andriotis A N, Menon M, Sheetz R M and Chernozatonskii L 2003 *Phys. Rev. Lett.* **90** 026801
[10] Kim Y H, Choi J, Chang K J and Tománek D 2003 *Phys. Rev.* B **68** 125420
[11] Banhart F 1999 *Rep. Prog. Phys.* **62** 1181
[12] Krasheninnikov A, Nordlund K and Keinonen J 2002 *Phys. Rev.* B **65** 165423
[13] Beuneu F, L'Huillier C, Salvetat J P, Bonard J M and Forró L 1999 *Phys. Rev.* B **59** 5945
[14] Likodimos V, Glenis S, Guskos N and Lin C L 2003 *Phys. Rev.* B **68** 045417
[15] Lu A J and Pan B C 2004 *Phys. Rev. Lett.* **92** 105504

Institute *of* **Physics** ⏀ DEUTSCHE PHYSIKALISCHE GESELLSCHAFT

[16] Kresse G and Furthmüller J 1996 *Comp. Mater. Sci.* **6** 15
[17] Kresse G and Furthmüller J 1996 *Phys. Rev.* B **54** 11169
[18] Perdew J P, Chevary J A, Vosko S H, Jackson K A, Pederson M R, Singh D J and Fiolhais C 1992
       Phys. Rev. B **46** 6671
[19] Kresse G and Joubert J 1999 *Phys. Rev.* B **59** 1758
[20] Blöchl P E 1994 *Phys. Rev.* B **50** 17953
[21] Monkhorst H J and Pack J D 1976 *Phys. Rev.* B **13** 5188
[22] Hult J R E, Hyldgaard P and Lundqvist B I 2001 *Phys. Rev.* B **64** 195414
[23] Hjort M and Stafström S 2000 *Phys. Rev.* B **61** 14089
[24] El-Barbary A A, Telling R H, Ewels C P, Heggie M I and Briddon P R 2003 *Phys. Rev.* B **68** 144107
[25] Telling R H, Ewels C P, El-Barbary A A and Heggie M I 2003 *Nature Mater.* **2** 333
[26] Qian G-X, Martin R M and Chadi D J 1988 *Phys. Rev.* B **38** 7649
[27] Thrower P A and Mayer R M 1978 *Stat. Sol.* A **47** 11
[28] Kaxiras E and Pandey K C 1988 *Phys. Rev. Lett.* **61** 2693
[29] Blase X, Benedict L X, Shirley E L and Louie S G 1994 *Phys. Rev. Lett.* **72** 1878
[30] Saito R, Fujita M, Desselhaus G and Dresselhaus M S 1998 *Physical Properties of Carbon Nanotubes*
       (London: Imperial College London Press)
[31] Ajayan P M, Ravikumar V and Charlier J-C 1998 *Phys. Rev. Lett.* **81** 1437
[32] Ouyang M, Huang J L, Cheung C L and Lieber C M 2001 *Science* **292** 702
[33] Cabria I, Mintmire J W and White C T 2003 *Phys. Rev.* B **67** 121406R
[34] Machón M, Reich S, Thomsen C, Sánchez-Portal D and Ordejón P 2002 *Phys. Rev.* B **66** 155410
[35] Kane C L and Mele E J 1997 *Phys. Rev. Lett.* **78** 1932
[36] Hamada N, Sawada S I and Oshiyama A 1992 *Phys. Rev. Lett.* **68** 1579
[37] Nakada K, Fujita M, Dresselhaus G and Dresselhaus M S 1996 *Phys. Rev.* B **54** 17954
[38] Kusakabe K and Maruyama M 2003 *Phys. Rev.* B **67** 092406
[39] Miyamoto Y, Nakada K and Fujita M 1999 *Phys. Rev.* B **59** 9858
[40] Tasaki H 1998 *Prog. Theor. Phys.* **99** 489
[41] Tonomura O, Mera Y, Hida A, Nakamura Y, Meguro T and Maeda K 2002 *Appl. Phys.* A **74** 311
[42] Kushmerick J G, Kelly K F, Rust H P, Halas N J and Weiss P S 1999 *J. Chem. Phys.* B **103** 1619
[43] Krasheninnikov A V 2001 *Solid State Commun.* **118** 361
[44] Krasheninnikov A V, Nordlund K, Sirviö M, Salonen E and Keinonen J 2001 *Phys. Rev.* B **63** 245405
[45] Kantorovich L N 2001 www.cmmp.ucl.ac.uk/∼lev